Galvanic Cell Type Humidity Sensor with NASICON-Based Material Operative at High Temperature

Shouhua Feng† and Martha Greenblatt*

Department of Chemistry, Rutgers, The State University of New Jersey, Piscataway, New Jersey 08855-0939

Received May 19, 1992. Revised Manuscript Received July 28, 1992

A galvanic cell type humidity sensor based on a proton-conducting NASICON ($HZr_2P_3O_{12}$) material was studied and characterized by powder X-ray diffraction, differential thermal analysis, and thermogravimetric analysis. Proton conductivity in the sensor material was confirmed by an ac impedance technique in the temperature range 350–600 °C. The electromotive force (emf) of the galvanic cell as a function of the partial pressure of water in a wide range, from 2 to 200 mmHg, was found to follow Nernstian behavior at ~450 °C. The response time of the emf to the change of water vapor pressure decreases from 50 to 6 s with increasing the temperature from 350 to 550 °C. The reproducibility and durability of the humidity sensor are excellent. The effects of some impurity gases (ethyl alcohol, acetic acid, and ammonia) and the operating temperature on the emf of the humidity sensor are presented.

1. Introduction

Solid electrolyte humidity sensors are widely used for controlling the environment in automatic industrial systems. Ideally, such sensors provide a direct electrical signal, e.g., potentiometric, amperometric, or conductimetric, as a function of humidity in the atmosphere. A galvanic cell (i.e., concentration cell) technique based on the measurement of electromotive force (emf) was first applied to a humidity sensor by Iwahara and co-workers.[1-3] Subsequently several humidity, hydrogen, and oxygen sensors based on this technique were reported.[4-7]

For galvanic cell type humidity sensor, a proton-conducting electrolyte as the humidity-sensing element is required. The emf behavior of such a cell ideally follows Nernstian behavior which serves as a calibration curve for the sensor. The appropriate humidity-sensing material (i.e., proton-conducting solid electrolyte) is considered to be the key factor for the development of such humidity sensors. Iwahara et al. were the first to use sintered $MCe_{1-x}Y_xO_3$ (M = Ba or Sr) perovskite-related phases for galvanic-type humidity sensors. Currently, the application of such perovskite-type solid electrolytes in high-temperature steam cells and fuel cells are being studied extensively.[8,9] However, electronic and/or oxide ion conduction in the $MCeO_3$-based oxides cause significant deviations from Nernstian behavior. In such cases, additional calibration is required. There are few humidity-sensing materials reported to date which are applicable at high temperatures. There is a need for humidity sensors operating at temperatures higher than 100 °C for many industrial applications. We have been investigating new materials, primarily proton-conducting solid electrolytes appropriate for humidity sensing at relatively high temperature. For example, sintered β-$Ca(PO_3)_2$ as a high-temperature humidity sensor was recently investigated in our laboratory.[10] However, this material appears to decompose in prolonged application above 650 °C.

It is well-known that NASICON materials ($Na_{1+x}Zr_2Si_xP_{3-x}O_{12}$) are fast sodium ion conductors.[11,12] The structure of both end members, i.e., x = 0 and 3 ($NaZr_2P_3O_{12}$ and $Na_4Zr_2Si_3O_{12}$, respectively) is composed of a rigid three-dimensional network lattice with interconnected cavities. In the phosphate analogue, the sodium ion occupies only one of the cavities. The proton-substituted NASICON, $HZr_2P_3O_{12}$ obtained from the calcination of $(NH_4)Zr_2P_3O_{12}$,[13-16] is a high-temperature proton-conducting material and is thermally stable up to 700 °C. Thus, $HZr_2P_3O_{12}$ is a possible candidate for high-temperature humiding sensing. Recently, Canaday et al. have reported on a phosphoric acid-bonded hydronium NASICON electrolyte as a hydrogen sensor at 25 °C as well as the effect of water vapor on the operation of this hydrogen sensor.[17-21]

†Present address: Department of Chemistry, Jilin University, Changchun, China.

*To whom correspondence should be addressed.

(1) Iwahara, H.; Esaka, T.; Uchida, H.; Maeda, N. *Solid State Ionics* **1981**, *3/4*, 359.

(2) Uchida, H.; Maeda, N.; Iwahara, H. *J. Appl. Electrochem.* **1982**, *12*, 645.

(3) Iwahara, H.; Uchida, H.; Kondo, J. *J. Appl. Electrochem.* **1983**, *13*, 365.

(4) Uchida, H.; Maeda, N.; Iwahara, H. *Solid State Ionics* **1983**, *11*, 117.

(5) Iwahara, H.; Uchida, H.; Maeda, N. *Solid State Ionics* **1983**, *11*, 109.

(6) Nagata, K.; Nishino, M.; Goto, K. S. *J. Electrochem. Soc.* **1987**, *134*, 1850.

(7) Inoue, T.; Seki, N.; Eguchi, K.; Arai, H. *J. Electrochem. Soc.* **1990**, *137*, 2523.

(8) Iwahara, H.; Uchida, H.; Maeda, N. *J. Power Sources* **1982**, *7*, 293.

(9) Iwahara, H.; Uchida, H.; Esaka, T. *Prog. Batteries Sol. Cells* **1982**, *4*, 279.

(10) Greenblatt, M.; Tsai, P. P.; Kodama, T.; Tanase, S. *Solid State Ionics* **1990**, *40/41*, 444.

(11) Goodenough, J. B.; Hong, H. Y.-P.; Kafalas, J. A. *Mater. Res. Bull.* **1976**, *11*, 203.

(12) Hong, H. Y.-P. *Mater. Res. Bull.* **1976**, *11*, 173.

(13) Clearfield, A.; Roberts, B. D.; Subramanian, M. A. *Mater. Res. Bull.* **1984**, *19*, 219.

(14) Subramanian, M. A.; Roberts, B. D.; Clearfield, A. *Mater. Res. Bull.* **1984**, *19*, 1471.

(15) Ono, A. *J. Mater. Sci.* **1984**, *19*, 2691.

(16) Rudolf, P. R.; Subramanian, M. A.; Clearfield, A. *Solid State Ionics* **1985**, *17*, 337.

(17) Gulens, J.; Longhurst, T. H.; Kuriakose, A. K.; Canady, J. D. *Solid State Ionics* **1988**, *28–30*, 622.

(18) Gulens, J.; Hildebrandt, B. W.; Canaday, J. D.; Kuriakose, A. K.; Wheat, T. A.; Ahmad, A. *Solid State Ionics* **1989**, *35*, 45.

(19) Canaday, J. D.; Kuriakose, A. K.; Wheat, T. A.; Ahmad, A.; Gulens, J.; Hildebrandt, B. W. *Solid State Ionics* **1989**, *35*, 165.

(20) Chehab, S. F.; Canaday, J. D.; Kuriakose, A. K.; Wheat, T. A.; Ahmad, A. *Solid State Ionics* **1991**, *45*, 299.

(21) Canaday, J. D.; Chehab, S. F.; Kuriakose, A. K.; Ahmad, A.; Wheat, T. A. *Solid State Ionics* **1991**, *48*, 113.

0897-4756/92/2804-1257$03.00/0

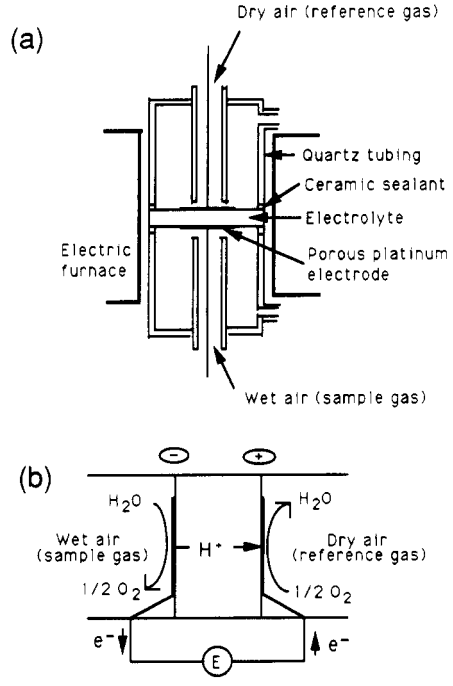

Figure 1. Schematic (a) and principle (b) illustration of test galvanic cell type humidity sensor.

In this paper, we report on the preparation and characterization of a humidity sensor based on a protonic NASICON conductor. A galvanic cell based on a $HZr_2P_3O_{12}/ZrP_2O_7$ composite humidity sensor was constructed and the emf behavior of the galvanic cell as a function of humidity was investigated in the temperature range 350–600 °C.

2. Experimental Section

Syntheses of Materials. $(NH_4)Zr_2P_3O_{12}$ was synthesized by a hydrothermal method in a stainless steel autoclave lined with poly(tetrafluoroethylene) (PTFE) from an aqueous mixture of $ZrOCl_2 \cdot 8H_2O$ (Aldrich Chemical Co., Inc.) and $(NH_4)H_2PO_4$ (Fisher Scientific; one volume of 1 M $ZrOCl_2 \cdot 8H_2O$ was added to 2 volumes of 1 M $(NH_4)H_2PO_4$)) according to a previous method.[13] Crystallization was carried out under autogenous pressure at 250 °C for 20 h. The crystalline product was filtered, washed with distilled water, and dried at ambient temperature. $HZr_2P_3O_{12}$ was prepared by heating $(NH_4)Zr_2P_3O_{12}$ in air at 650 °C for 5 h. α-ZrP ($Zr(HPO_4)_2 \cdot H_2O$) was synthesized according to the procedure described in ref 22.

Preparative Procedure for the Sensor Electrolyte. Powdered $HZr_2P_3O_{12}$ (HZP) was first mixed with α-$Zr(HPO_4)_2 \cdot H_2O$ (ZrP) in a HZP/ZrP mole ratio of unity to form a HZP–ZrP mixture. The mixture was thoroughly ground and then pelletized (1.0 cm in diameter and 0.2 cm in thickness) with a pressure of 150 klb/in.^{2}. The resulting pellet was sintered in air at 600 °C for 10 h. The observed density of the sintered pellet was greater than 80% of the ideal. Electrode connections were made by coating both faces of the pellet with platinum ink (electrode area ~0.2 cm^2). Finally the pellet with Pt electrodes was heat treated at 600 °C for 10 h to form a sensor disk.

Structural Characterization. The powder X-ray diffraction (XRD) patterns were recorded on a Scintag X-ray diffractometer using monochromatized Cu Kα radiation. Differential thermal and thermogravimetric analyses (DTA and TGA) were carried out on a Du Pont Model 9900 thermal analyzer with a heating rate of 10 °C/min in air.

Ac Impedance Analysis. Ionic conductivities were measured by an ac impedance technique using a Solartron Model 1250 frequency analyzer and 1186 electrochemical interface that were equipped with a Hewlett-Packard 9816 desktop computer for data collection and analysis. To keep the water content in all the samples identical for the ac impedance measurement, samples were preheated at 600 °C for 1 h and then placed in a desiccator at room temperature over a NH_4Cl-saturated solution for 72 h prior to measurement. A frequency range from 10 Hz to 65 kHz and a heating rate of 2 °C/min were used throughout.

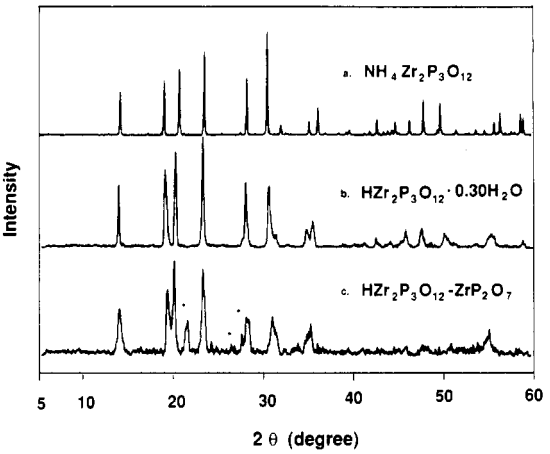

Figure 2. XRD pattern of pure (a) $(NH_4)Zr_2P_3O_{12}$, (b) $HZr_2P_3O_{12}$, and the sensor composite HZr_2P_{O12}/ZrP_2O_7 (c).

EMF Measurement. Details of the galvanic cell and the emf measurements were reported previously.[10] The schematic of a humidity-controlled galvanic cell is illustrated in Figure 1a. Humidity is introduced to both sample and reference compartments from water reservoirs with air as the carrier gas at a flow rate of 220 cm^3/min. The humidity in the reference compartment is fixed at 3.16 mmHg by maintaining the reference water reservoir in an ice bath. The humidity in the sample compartment is varied by changing the temperature of the sample reservoir. The galvanic cell assembly is represented by the following components:

Pt, H_2O (reference gas in air)/solid electrolyte/
H_2O (sample gas in air), Pt

For a proton-conducting solid electrolyte as in Figure 1b, when the pressure of water vapor in the two compartments is different, the electrode reactions are

$$H_2O = 2H^+ + \tfrac{1}{2}O_2 + 2e^- \quad \text{at anode} \tag{1}$$

$$2H^+ + \tfrac{1}{2}O_2 + 2e^- = H_2O \quad \text{at cathode} \tag{2}$$

The equilibrium partial pressure of water in the concentration cell is expressed by the Nernst equation:

$$E = RT/2F \ln [P_{H_2O}(P^r_{O_2})^{1/2}/P^r_{H_2O}(P_{O_2})^{1/2}] \tag{3}$$

$$P_{H_2O} = P^r_{H_2O}(P_{O_2}/P^r_{O_2})^{1/2} \exp(2EF/RT) \tag{4}$$

where $P^r_{H_2O}$ and $P^r_{O_2}$ are the partial pressures of water and oxygen respectively at the reference electrode, E is the electromotive force of the electrolyte, F and R are the Faraday constant and gas constant, respectively. Under ambient atmospheric conditions, P_{O_2} is assumed to be equal to $P^r_{O_2}$, and then for sensing applications the partial pressure of water vapor in the sample gas, P_{H_2O} can be estimated from the emf of the cell:

$$E = RT/2F \ln (P_{H_2O}/P^r_{H_2O}) \tag{5}$$

$$P_{H_2O} = P^r_{H_2O} \exp(2EF/RT) \tag{6}$$

3. Results and Discussion

3.1. Preparation of the Humidity-Sensing Electrolyte. For a galvanic cell type humidity sensor, bulk ionic conductivity and a dense ceramic body of the electrolyte are required (Figure 1). Since synthetic protonic NASICON, $HZr_2P_3O_{12}$ could not be sintered to high density, a very fine powder (~100–1000 Å in diameter) of $Zr(HPO_4)_2 \cdot H_2O$ consisting of prismatic platelet shape crystallites was used as a binder in the ratio of HZP/ZrP

(22) Alberti, G.; Torracca, E. *J. Inorg. Nucl. Chem.* **1968**, *30*, 317.

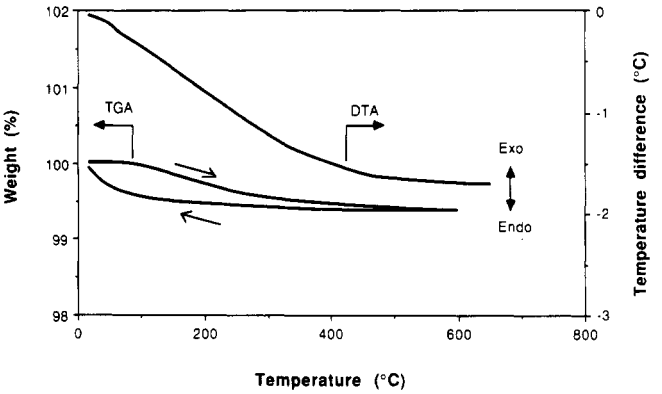

Figure 3. DTA and TGA curves of the sensor material, $HZr_2P_3O_{12}/ZrP_2O_7$.

= 1 to obtain a dense ceramic pellet as described above. The platelet morphology of the binder probably enhances good mechanical bonding between HZP and ZrP and the formation of a dense pellet before sintering. The sintered compact is a composite phase of $HZr_2P_3O_{12}$ and ZrP_2O_7 (ZP), as confirmed by XRD. ZrP_2O_7 is formed from $Zr(HPO_4)_2 \cdot H_2O$ during sintering. The humidity sensing element is a sintered, mechanically stable composite ceramic disk.

3.2. X-ray Diffraction Analysis. Figure 2 shows XRD patterns of $(NH_4)Zr_2P_3O_{12}$, $HZr_2P_3O_{12}$, and the sensor material. Hydrothermally synthesized $(NH_4)Zr_2P_3O_{12}$ has a high crystallinity (Figure 2a). Its framework structure is identical with that of the high-temperature phase of NASICON.[16,23] $HZr_2P_3O_{12}$ or $HZr_2P_3O_{12} \cdot xH_2O$ (x = 0–0.5) has two polymorphs, depending on the calcination temperature of $(NH_4)Zr_2P_3O_{12}$. Below 600 °C, a proposed triclinic phase and above 600 °C a rhombhedral phase are obtained.[13] The rhombohedral phase does not undergo a phase transition upon cooling or heating. Although we found that the triclinic phase has a somewhat higher proton conductivity than the rhombohedral phase and that each of the two phases responds to changes of humidity, we used the rhombohedral HZP (Figure 2) as the starting material for the sensor, because of its stability at high temperature. The XRD pattern of the sensor material shown in Figure 2c, is identical with that of rhombohedral $HZr_2P_3O_{12}$, except for a few additional peaks due to ZrP_2O_7. Thus the sensor material is a composite of $HZr_2P_3O_{12}$ and ZrP_2O_7. The ZrP_2O_7 is an effective binder, because it is formed in the sintering process. It is likely that cubic ZrP_2O_7 is bonded to $HZr_2P_3O_{12}$ particles in the grain boundary regions.

3.3. DTA and TGA. The DTA curve for a sample of the sensor material (Figure 3) shows no phase change in the temperature range of measurement and demonstrates the thermal stability of the sample upon heating and cooling. The DTA curve slopes smoothly from the beginning to the end of temperature range measured upon heating, indicating a gradual endotherm. A gradual weight loss was also indicated upon heating by TGA in Figure 3. A weight loss of 0.75% is attributed to loss of water, which was adsorbed by the sample on exposure to air (in this case at 25 °C for 2 h, corresponding to a formula, $HZr_2P_3O_{12} \cdot ZrP_2O_7 \cdot 0.15H_2O$). The amount of weight loss varied with the time of exposure to air. The TGA cooling curve for the same sample shows a weight gain, starting at ~400 °C. This is due to the reversible adsorption of water at relatively low temperature, which was confirmed by heating and cooling cycle experiments of the TGA.

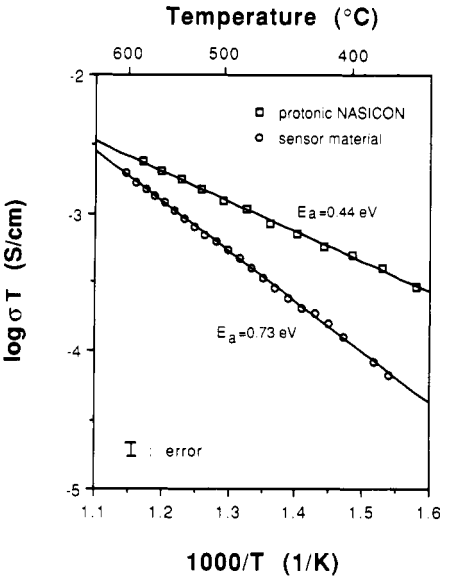

Figure 4. Arrhenius plots of proton conductivity of $HZr_2P_3O_{12}$ and the sensor material $HZr_2P_3O_{12}/ZrP_2O_7$ in air.

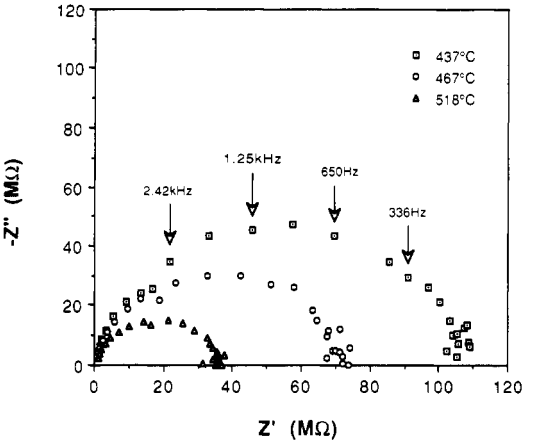

Figure 5. Variation of ac impedance of the sensor material at 437, 467, and 518 °C.

3.4. Ac Impedance Measurements: Proton Conductivity. Figure 4 shows Arrhenius plots of proton conductivity obtained from complex impedance spectra measured at different temperatures for $HZr_2P_3O_{12}$ and the sensor material in air. The temperature dependence of conductivity of both samples is linear in the temperature range of measurement. The activation energy of the sensor material (0.73 eV) is higher than that of $HZr_2P_3O_{12}$ (0.44 eV). This is probably due to the nonconducting ZrP_2O_7 phase in the conducting $HZr_2P_3O_{12}$ material. The ac impedance spectra (Figure 5) of the sensor material at 437, 467, and 518 °C, respectively are single semicircles in the frequency range measured, indicating bulk character of proton conductivity. We noted that the proton conductivity in both samples is strongly dependent on the water content initially adsorbed in the samples.[24] The ac impedance conductivity cooling curves did not coincide with those of the heating curves due to the loss of water in the sample at high temperature.

3.5. EMF Response to Water Vapor Pressure. Figure 6 shows the emf response of the galvanic cell as a function of the logarithm of the partial pressure of water

(23) Kreuer, K.-D.; Kohler, H.; Maier, J. *High Conductivity Ionic Conductors: Recent Trends and Application*, Takahashi, T., Ed.; World Scientific Publishing Co.: Singapore, 1989; p 242.

(24) Feng, S.; Greenblatt, M., submitted for publication.

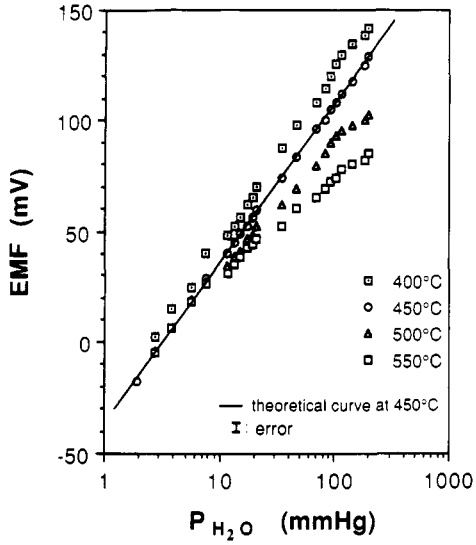

Figure 6. Humidity dependence of emf of sensor at 400, 450, 500, and 550 °C.

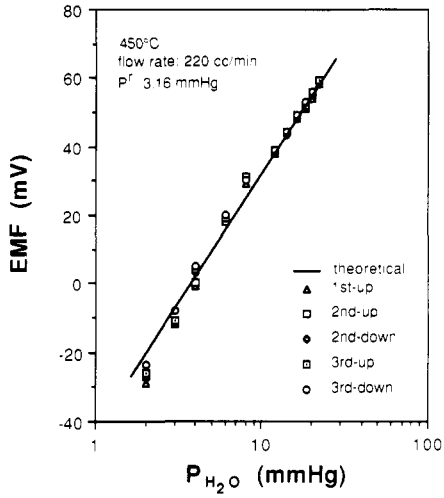

Figure 7. Humidity dependence of emf of sensor at 450 °C showing cycling data.

in the sample compartment at 400–550 °C. In the temperature range 425–525 °C, this cell gives a stable emf over the entire P_{H_2O} range examined (2–200 mmHg). The EMF vs log P_{H_2O} is linear, and the measured emf's are in good agreement with the theoretical values, E, calculated from eq 5 for 450 °C (the solid line). The cell gives rise to reproducible emf values in response to change in the water vapor pressure. Testing of the cell at 500 °C over a 2-month period (Figure 7) gave reproducible emf results which demonstrates the durability of the sensor material.

Below and above 450 °C, deviation of emf from Nernstian behavior was observed, although the variation of EMF vs log P_{H_2O} was still more or less linear. Figure 6 shows that at <450 °C the EMF values are higher, and at >450 °C the emf values are lower than expected from Nernst equation and are nonlinear. A plausible reason for the voltage deviation at lower temperature (<450 °C) may be due to adsorption of water on the surface of the sensor disk, as also seen in the TGA cooling curve in Figure 3. It was shown that the mechanism of proton migration in protonic NASICON depends on the initial water content in the structure.[18] More water molecules in the structure result in higher conductivity and lower activation energy for proton conduction. Thus water adsorption results in a change of the proton transport mechanism. Above 450 °C the sample shows significant proton conductivity even

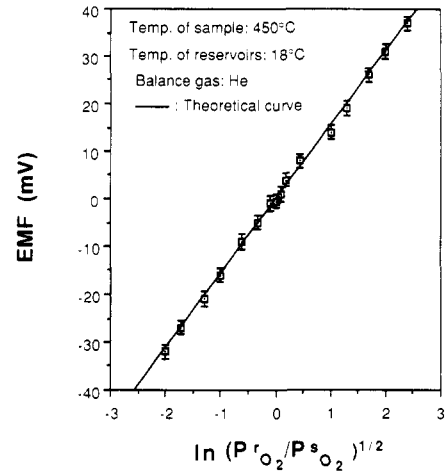

Figure 8. Relationship between observed emf and ratio of the partial oxygen pressures in reference and sample compartments. The atmosphere in both compartments was moistened using a water reservoir kept at a temperature of 18 °C, corresponding to 15.5 mmHg of the water vapor pressure.

without water (Figure 4). These intrinsic protons do not contribute to the emf; moreover, they probably supress the formation of H^+ indicated by the reaction in eq 1, leading to the reduced values of emf observed at $T > 450$ °C.

The conduction characteristics of the sensor material were further investigated using a wet oxygen concentration cell with the same partial pressures of water vapor in both sample and reference compartments. The partial pressures of oxygen in both sample and reference compartments were adjusted from 68 to 745 mmHg with He balance gas. The measured emf's at 450 °C of the wet oxygen concentration cell with changing oxygen concentration follow the theoretical values exactly as calculated from eq 3 (Figure 8). This result provides evidence that the sensor material operates in the concentration cell by a mechanism according to eqs 1 and 2.

The response time of the sensor as a function of temperature on changing P_{H_2O} is shown in Figure 9a. As the humidity is varied, the EMF responds rapidly and reaches a steady state within a few seconds at all temperatures examined. At 350 °C, the response time is 48 s; however, the response time is significantly shortened at elevated temperatures; at 450 °C, the response time is within 15 s (Figure 9b). The response time may be affected by the volume of the humidity compartment as well as the flow rate.

3.6. Effect of Impurity Gases on the EMF. The effect of selected impurity gases in the water vapor, such as ethyl alcohol (C_2H_5OH), acetic acid (CH_3CH_2COOH), and ammonia (NH_3) on the emf of the sensor were examined. Pure C_2H_5OH, CH_3CH_2COOH, and NH_3 were mixed with water in a volume ratio of 100 or 1000 ppm. The solution mixture served as the source of saturated water vapor plus impurity vapor supplied to the sample compartment. The sensor material is stable against each of these impurity gases, and the humidity sensing was not affected within the experimental error of measurement for 100 ppm impurity gas concentration. This shows reasonable selectivity of the sensor material. When the concentration of any of the impurity gas was greater than 100 ppm, the value of emf increased, as shown in Figure 10.

Increased impurity gas concentrations affected the emf value even at relatively low temperature (450 °C). For example, at 450 °C the EMF appears to be dependent upon the C_2H_5OH concentration for values above 100 ppm, as shown in Figure 11. This phenomenon may be at-

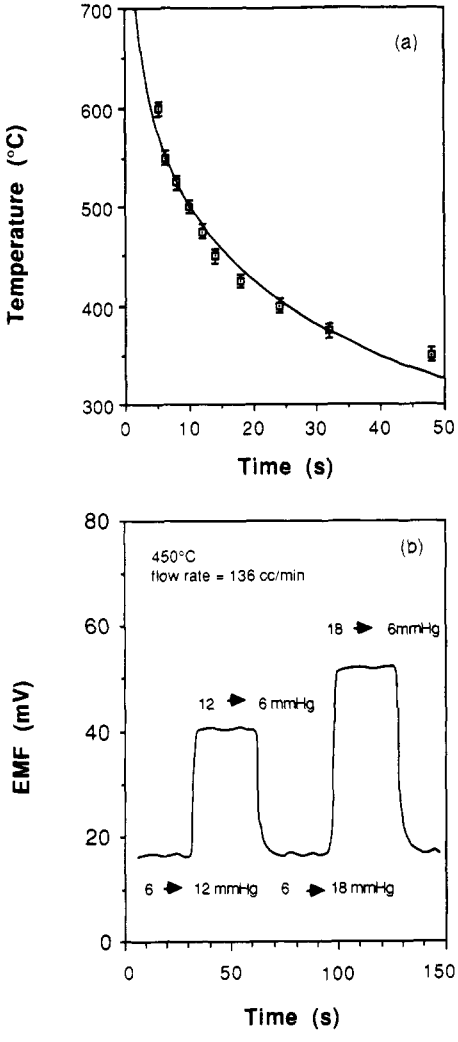

Figure 9. (a) Temperature dependence of response time for the humidity sensor with the change of partial pressure of water from 6 to 18 mmHg and (b) variation of emf with time of the cell with change of partial pressure of water from 6 to 12 mmHg and from 6 to 18 mmHg at 450 °C.

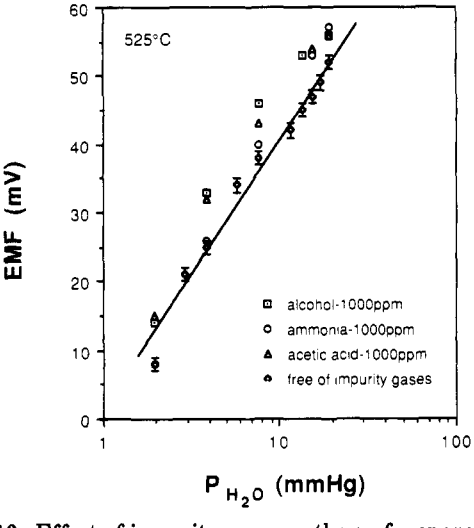

Figure 10. Effect of impurity gases on the emf response of the galvanic cell at 525 °C; the water vapor pressure introduced in the reference compartment is 3.16 mmHg; the flow rate is 220 cm^3/min. The solid line represents the emf value of the sample in pure water vapor.

tributed to proton reactivity of the C_2H_5OH molecules. The C_2H_5OH molecules are adsorbed on the surface of the sensor disk in the sample compartment and could provide additional protons, which result in the enhanced emf observed. These results suggest possible applications of the humidity sensing material as a proton-containing gas sensor and/or catalyst.

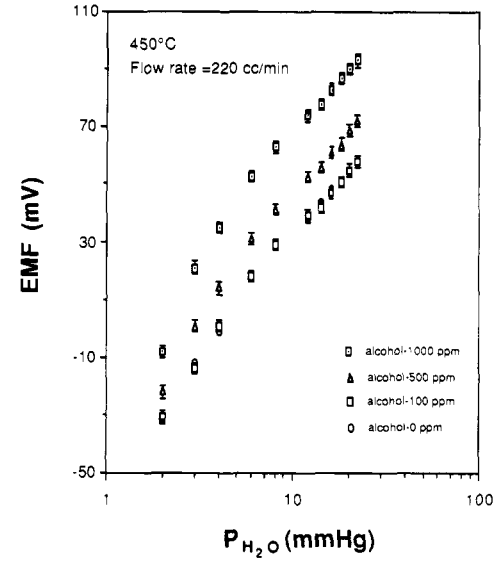

Figure 11. Effect of ethyl alcohol content on the EMF response at 450 °C.

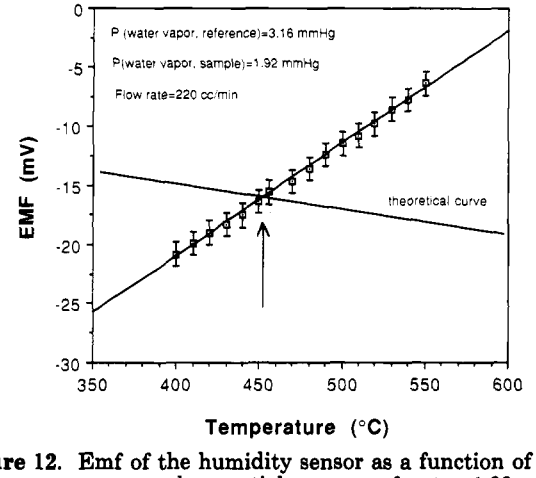

Figure 12. Emf of the humidity sensor as a function of temperature at a constant low partial pressure of water, 1.92 mmHg in both compartments; the intersection temperature of the experimental and theoretical curves is at ~450 °C.

3.7. Operation Temperature. Figure 12 shows the temperature dependence of the emf at a constant water vapor pressure of 1.92 mmHg in the sample compartment and 3.16 mmHg in the reference compartment (Figure 1a). When $P^r_{H_2O} > P_{H_2O}$, the value of the emf measured is negative. We can see that only at ~450 °C are the experimental values of emf close to the theoretical points (intersection of two lines in Figure 12). The theoretical curve has a negative slope, while the experimental curve has a positive slope. Below and above 450 °C the experimental values of emf are lower and higher respectively than those of the theoretical emf. This observation is not in contradiction of the apparently opposite effect we discussed in section 3.5, because in Figure 6 $P^s_{H_2O} > P^r_{H_2O}$.

To clarify our results, we examined the background emf (i.e., no water vapor was introduced into sample and reference compartments) of the sensor. The data (see Figure 13) show a minimum value of emf at about 450 °C. The magnitude of the emf mainly reflects the intrinsic character of the sensor material. This suggests an optimal operating

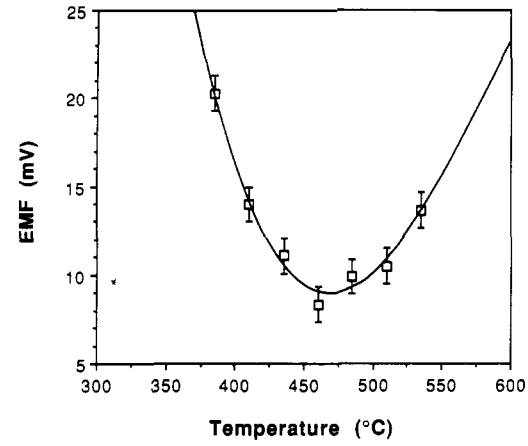

Figure 13. Variation of the background emf with temperature without any water vapor pressure in sample and reference compartments; the conditions on both sides of the sensor are identical (i.e., air at atmospheric pressure); the minimum in the background EMF is at ~450 °C.

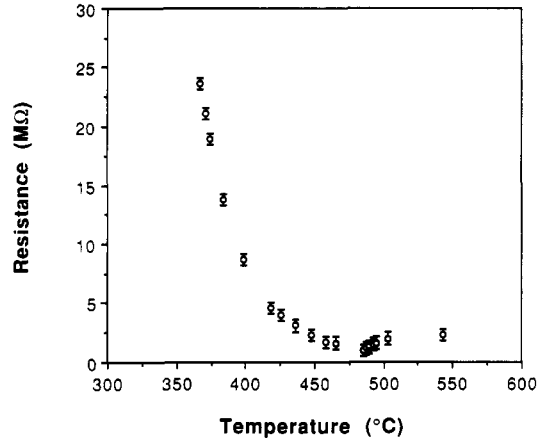

Figure 14. Temperature dependence of the dc resistance of the sensor; no water vapor was present; the conditions on both sides of the sensor are identical; the minimum in the resistance is ~450 °C.

temperature range, where the effect of temperature on the sensor material is smallest. A similar phenomenon was observed in examining the temperature dependence of resistance (measured by a dc method, i.e., open-circuit potential) of the sensor sample, as shown in Figure 14. A minimum region of resistance in the sample, at around 450 °C, is observed. Thus, the sample in this temperature region has the lowest resistance, which is consistent with the lowest background in the EMF in this temperature range. Although the galvanic cell itself and its electronic circuit system may affect the data obtained here, these experimental observations are in agreement with an optimal operation temperature being at ~450 °C for the $HZr_2P_3O_{12}/ZrP_2O_7$ humidity-sensing material.

4. Conclusions

In summary, a galvanic cell type humidity sensor based on a dense ceramic composite of $HZr_2P_3O_{12}$ and ZrP_2O_7 (the latter served as a binder) has been characterized. Ac impedance spectroscopy indicates ionic conductivity of the sensor composite (σ(450 °C) ~ 10^{-5} S cm^{-1}; E_a ~ 0.73 eV), which greatly depends on the initial water content of the material. For the galvanic cell, the temperature dependence of emf as a function of water vapor pressure follows Nernstian behavior reproducibly upon cycling at ~450 °C, for long periods of time. The response time at the optimal temperature of operations (450 °C) is 15 s. The variation of emf with oxygen pressure in a wet oxygen concentration cell (i.e. P_{H_2O} is positive and the same in both sample and reference compartments) also follows Nernstian behavior, which confirms the proposed mechanism of proton conductivity in the composite $HZr_2P_3O_{12}/ZrP_2O_7$ electrolyte sensor. Selected impurity gases, including ethanol, acetic acid and ammonia with less than 100 ppm concentration do not affect the value of emf of this galvanic cell type humidity sensor.

Acknowledgment. We thank Prof. W. H. McCarroll for critical reading of the manuscript and useful suggestions for improving it. This is publication No. D10551-7-91 of the New Jersey Agricultural Experiment Station supported by State Funds and the Center for Advanced Food Technology (CAFT). The Center for Advanced Food Technology is a New Jersey Commission on Science and Technology Center.

Registry No. EtOH, 64-17-5; CH_3CO_2H, 64-19-7; NH_3, 7664-41-7; nasicon, 77641-62-4.